

TCE Dechlorination Rates, Pathways, and Efficiency of Nanoscale Iron Particles with Different Properties

YUEQIANG LIU,[†] SARA A. MAJETICH,[‡]
ROBERT D. TILTON,[§]
DAVID S. SHOLL,[§] AND
GREGORY V. LOWRY^{*,†}

Department of Civil & Environmental Engineering,
Physics Department, and Department of Chemical
Engineering, Carnegie Mellon University,
Pittsburgh, Pennsylvania 15213-3890

Nanoscale Fe⁰ particles are a promising technology for in situ remediation of trichloroethene (TCE) plumes and TCE-DNAPL source areas, but the physical and chemical properties controlling their reactivity are not yet understood. Here, the TCE reaction rates, pathways, and efficiency of two nanoscale Fe⁰ particles are measured in batch reactors: particles synthesized from sodium borohydride reduction of ferrous iron (Fe/B) and commercially available particles (RNIP). Reactivity was determined under iron-limited (high [TCE]) and excess iron (low [TCE]) conditions and with and without added H₂. Particle efficiency, defined as the fraction of the Fe⁰ in the particles that is used to dechlorinate TCE, was determined under iron-limited conditions. Both particles had a core/shell structure and similar specific surface areas (~30 m²/g). Using excess iron, Fe/B transformed TCE into ethane (80%) and C3–C6 coupling products (20%). The measured surface area normalized pseudo-first-order rate constant for Fe/B ($1.4 \times 10^{-2} \text{ L}\cdot\text{h}^{-1}\cdot\text{m}^{-2}$) is ~4-fold higher than for RNIP ($3.1 \times 10^{-3} \text{ L}\cdot\text{h}^{-1}\cdot\text{m}^{-2}$). All the Fe⁰ in Fe/B was accessible for TCE dechlorination, and $92 \pm 0.7\%$ of the Fe⁰ was used to reduce TCE. For Fe/B, H₂ evolved from reduction of water (H⁺) was subsequently used for TCE dechlorination, and adding H₂ to the reactor increased both the dechlorination rate and the mass of TCE reduced, indicating that a catalytic pathway exists. RNIP yielded unsaturated products (acetylene and ethene). Nearly half (46%) of the Fe⁰ in RNIP was unavailable for TCE dechlorination over the course of the experiment and remained in the particles. Adding H₂ did not change the reaction rate or efficiency of RNIP. Despite this, the mass of TCE dechlorinated per mass of Fe⁰ added was similar for both particles due to the less saturated products formed from RNIP. The oxide shell composition and the boron content are the most likely causes for the differences between the particle types.

Introduction

Chlorinated solvents such as trichloroethene (TCE) that are present in the subsurface as nonaqueous phase liquids (NAPL) are continuous long-term sources of halogenated

organic contaminants (HOCs) to groundwater. Removing these sources can speed up remediation and reduce the time to site closure, but reliable cost-effective methods to remediate NAPL-impacted sites are needed. For more than a decade, iron filings have been used in permeable reactive barriers to effectively treat HOC-contaminated groundwater plumes emanating from NAPL source areas. The rates and pathways of TCE dechlorination by iron filings have been intensively studied and are fairly well understood. In the reaction between TCE and iron filings, TCE is reduced and releases chloride ions, while iron is oxidized and supplies electrons (1–5). The proposed reaction pathways are β -elimination (primary), hydrogenolysis (minor), and hydrogenation (minor). These mechanisms explain the formation of ethene and ethane as the main products, with minor amounts of chlorinated intermediates (formed via hydrogenolysis) and acetylene (formed via β -elimination) (3–6). Iron oxides and oxyhydroxides on the particle's surface mediate these reactions (7–9), but the exact nature of how different iron oxide phases affect the rate and products formed remains unclear.

Recently, nanoscale iron and bimetallic (Pd–Fe and Ni–Fe) particles have been used for in situ TCE dechlorination. For example, Elliott and Zhang (10) successfully injected bimetallic (Pd–Fe) nanoparticles into a sand aquifer to remediate a dissolved TCE plume. Nanoscale iron has also been delivered to a TCE NAPL source area using a water/vegetable oil/surfactant emulsion (11). These studies demonstrate that nanoparticles can be delivered in situ; however, it has also been shown that their small size alone is not sufficient to ensure adequate transport in the subsurface, and effective delivery mechanisms are still needed (12).

Recent research has focused on bimetallic (Fe–Pd and/or Fe–Ni) nanoscale particles (10, 13–19). They have much higher TCE dechlorination rates than iron filings and typically provide saturated hydrocarbon products (e.g., ethane). Their high surface to volume ratio and the addition of a catalyst are reported to be the cause of the increased reactivity relative to iron filings. The Pd or Ni alloys formed on the particle surfaces also oxidize less rapidly than Fe⁰ and preserve the Fe⁰ core for TCE dechlorination. A core/shell model has been proposed, where the shell is an iron oxide with embedded catalyst (Ni or Pd) and the core is Fe⁰. Electrons from oxidation of the Fe⁰ core are transported through the iron oxide/catalyst shell to reduce adsorbed TCE (16). Bimetallic iron particles effectively degrade TCE, but they may themselves pose an environmental risk by introducing undesirable metals (e.g., Ni) into the subsurface.

Less is known about the reaction kinetics and products formed during TCE dechlorination by iron nanoparticles without a catalyst metal. The reported surface area normalized TCE reaction rates by nanoscale iron ($2\text{--}3 \times 10^{-3} \text{ L}\cdot\text{h}^{-1}\cdot\text{m}^{-2}$) (13, 16) are similar to or slightly higher than those for iron filings ($\sim 10^{-4}\text{--}10^{-3} \text{ L}\cdot\text{h}^{-1}\cdot\text{m}^{-2}$) (20), but their significantly larger specific surface area makes them attractive for field application. As with iron filings, non-chlorinated hydrocarbons (C2–C5) were observed as the final products from TCE degradation by nanoscale iron (13, 16), but details of the product distribution and reaction kinetics have not been described, and it is not clear if nanoscale iron dechlorinates TCE through the same pathways as iron filings. Reported TCE dechlorination pathways by iron filings are shown in Figure 1. This summary includes the observed products from β -elimination (pathway 2) and hydrogenolysis (pathway 1) using iron filings (5). Intermediate compounds (e.g., chloroacetylene, dichloroethenes, and vinyl chloride)

* Corresponding author phone: (412)268-2948; fax: (412)268-7813; e-mail: glowry@cmu.edu.

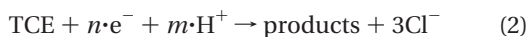
[†] Department of Civil & Environmental Engineering.

[‡] Physics Department.

[§] Department of Chemical Engineering.

are not included. A direct pathway from TCE to ethane reported for Pd-catalyzed TCE dechlorination (pathway 4) is also included (21). A direct pathway does not necessitate new pathways than those reported for iron, if for example, the intermediate compounds do not desorb from the particle surface before complete reduction to ethane and are not observed.

The mass of nanoscale iron needed for remediation depends, in part, on the fraction of the Fe⁰ in the particle core that is available for reaction. Given the small primary particle size in nanoscale Fe⁰ (~50 nm diameter), it is possible that all of the Fe⁰ in the core of the particles may be available for reaction, but the extent of utilization of Fe⁰ in the particles has not been evaluated. The mass of iron needed also depends on selectivity of the reaction for TCE dechlorination. In this study, the following half-reactions are of interest:



Electrons from Fe⁰ oxidation can be used to dechlorinate TCE (eq 2) or used to produce H₂ (eq 3). The mass of TCE dechlorinated per mass of Fe⁰ will depend on the relative rates of each of these reactions, on the value of *n* in eq 2 (which is a function of the product distribution), and on the accessibility of the Fe⁰ in the core of the particle. It also depends on the ability of the Fe⁰ particles to use the H₂ produced for reducing TCE. It has been reported that H₂ gas is evolved from nanoscale iron in water (16), but it remains unclear what factors influence the rate of H₂ produced, or if the H₂ generated can be used to reduce TCE.

Several methods are available to synthesize iron nanoparticles, but particles synthesized by aqueous phase reduction of ferrous or ferric iron by sodium borohydride (Fe/B) have been the most thoroughly investigated (10, 13–19). A second less studied type of iron nanoparticle, reactive nanoscale iron particles (RNIP), synthesized by gas-phase reduction of iron oxides in H₂ are commercially available from Toda Kogyo Corporation, Onoda, Japan (22). The ease of manufacturing and the lower cost of RNIP make them attractive for in situ remediation of TCE-impacted sites, but it is unclear if these particles can dechlorinate TCE as effectively as Fe/B. The physical and chemical properties affecting particle reactivity (e.g. iron oxide phase and boron content) are also unknown. In this study, the iron oxide phases and morphology of both particle types are determined using transmission electron microscopy (TEM), electron diffraction (ED), X-ray diffraction (XRD), and electron energy loss spectroscopy (EELS). The reaction rates and products formed from TCE dechlorination by each particle type are measured. The selectivity for TCE reduction over H₂ evolution and the influence of H₂ on TCE reactivity are also evaluated. The overall objective is to better understand the factors affecting the reactivity and efficiency of nanoscale Fe⁰ particles during TCE dechlorination. The specific research objectives are to (i) quantify the reaction rates and products formed from the different nanoparticles and determine the primary differences between the two particle types, (ii) determine the fraction of the Fe⁰ in the particle core that is available for reaction with TCE (efficiency), (iii) determine if the byproduct H₂ can be used to dechlorinate TCE, and (iv) gain insight into how the physical and chemical properties (e.g., iron oxide phases and thickness) affect the TCE reaction rates and pathway.

Materials and Methods

Chemicals. Ferrous sulfate (FeSO₄·7H₂O) (99.7%), sodium borohydride (NaBH₄) (98+%), and concentrated HCl (37%)

were supplied by Fisher Scientific. Amorphous B powder was purchased from Alfa Aesar. TCE (99.5+%), *cis*-1,2-dichloroethene (c-DCE) (98%), *trans*-1,2-dichloroethene (t-DCE) (98%), and 1,1-dichloroethene (1,1-DCE) (99%) were purchased from Aldrich. Methanol (histological grade) was purchased from Acros. Olefin standards (1000 ppm of ethene, propene, butene, pentene, and hexene), paraffin standards (1020 ppm of methane, ethane, propane, butane, pentane, and hexane), acetylene (1000 ppm, 1%), ethene (1%), ethane (1%), vinyl chloride (VC) (10 ppm), and hydrogen (1%) were obtained from Alltech. The balance of each was N₂, and all had ±2% variation. Ultrahigh purity argon and compressed N₂ were purchased from Butler Gas Products (Pittsburgh, PA).

Particle Preparation. Fe/B was synthesized by reduction of an aqueous phase ferrous iron solution by sodium borohydride using a slightly modified method than previously reported by Ponder et al. (18). FeSO₄·7H₂O was dissolved into a 30% (volume) methanol/deionized (DI) water solution, and 10 mL of 5 N NaOH aqueous solution was added dropwise to the dissolved iron solution yielding a pH of 6.1. Next, 50 mL of a 2.1 M NaBH₄ aqueous solution was added at a rate ~0.5 mL/s. The resulting particle suspension was centrifuged, and the separated Fe⁰ particles were dried under N₂ at 105 °C for 3–4 h. Air was allowed to bleed into the oven slowly overnight to stabilize the particles. Particles were subsequently stored in argon prior to use. Complete details of the synthesis method are provided in the Supporting Information. RNIP was obtained from Toda Kogyo Corp. (Onoda, Japan). The particles were shipped and stored in water (pH 10.6). Before use, the particles were dried in water under vacuum.

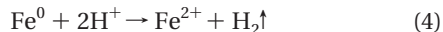
Batch Reactors. Batch experiments were conducted in 160 mL serum bottles capped by Teflon Mininert valves. The reactors were prepared in an anaerobic glovebox (argon) or a H₂-filled glovebag and contained 100 mL of deoxygenated water, 60 mL of headspace, and a specified mass of Fe⁰ particles and TCE. Either a saturated TCE solution or pure phase TCE was added to provide the desired initial TCE concentration. The reactors were rotated on an end-over-end rotator at 30 rpm at 22 ± 1 °C.

Analytical. Reactor headspace samples (100 μL) were analyzed on a HP 6890 GC equipped with a GS-Q plot column (30 m × 0.53 mm, Alltech) and a FID detector. Samples were injected splitless at 250 °C. The oven temperature program (50 °C for 2 min, ramp 40 °C/min to 220 °C, and hold for 6min) provided adequate separation between TCE and all chlorinated and non-chlorinated reaction products. When high concentrations of acetylene were present, ethane appeared as a shoulder on the acetylene peak. In these cases, the peaks were deconvolved to determine the ethane and acetylene concentrations. TCE calibration standards were prepared in the 160 mL reactors with the same water/headspace volume ratio as the reactors (100/60). DCE standards (c-, t-, 1,1-) were prepared in smaller (14 mL) reactors. Aqueous concentrations of TCE and its reaction products were calculated using reported Henry's constants (23–25). The carbon mass balance was calculated using the total measured mass of TCE and products and the initial mass of TCE added to the system.

For iron-limited conditions, the H₂ concentration in the reactors was also monitored. H₂ evolved from particles in deoxygenated DI water (no TCE) was measured using 200 mg/L of the Fe/B or 500 mg/L of RNIP. H₂ was quantified on a Shimadzu GC-14A equipped with a 1/8 in. o.d. × 10 m long HayeSep D (Alltech) packed column and a thermal conductivity detector (TCD). Argon (13 mL/min) was used as the carrier gas. The inlet temperature was 120 °C, the oven was isothermal at 30 °C, and the TCD was 120°C. Standards ranging from 0.25% to 5% hydrogen in headspace were used for calibration.

Iron Characterization. The iron particle sizes and electron diffraction patterns were collected using a Philips EM420 transmission electron microscope (TEM) at 120 kV. The morphology was further evaluated using the JEM-ARM 1000 atomic resolution microscope (JEOL, Ltd.) at the National Center for Electron Microscopy (Berkeley, CA). The ARM was operated at 800 kV, which allowed magnification levels of up to 1 000 000 \times . The distribution of oxygen atoms in the particles was examined using a Philips CM200/FEG operated at 200 kV and capable of electron energy-loss spectroscopy (EELS). Particles were dispersed (sonicated) in hexane or toluene and then dripped onto a 300 mesh Cu TEM grid coated with Formvar or lacey carbon. X-ray diffraction (XRD) of dried RNIP before and after reactions were performed on a Rigaku Geigerflex XRD with Cu K α X-ray source. Fe⁰ and oxide phases were identified by matching at least two spectrographic peaks from 2 θ 10–80°. The N₂-BET specific surface area of the particles was measured (5-point isotherm) using a NOVA 2200 BET-surface area analyzer (Quantachrome, Boynton Beach, FL). The boron content of the Fe/B was determined by inductively coupled plasma-atomic emission spectrometry (ICP-AES) according to EPA Method 6010B.

The Fe⁰ content in particles before and after reaction with TCE was determined by measuring the H₂ gas evolved during particle digestion in a concentrated HCl solution (37%). It was verified that amorphous B⁰ alone did not produce any H₂ under these conditions. On the basis of the reported standard reduction potentials, iron oxides (2) or B-oxides will not produce H₂ when acidified. It is unclear if an Fe⁰-B⁰ alloy can produce H₂ in HCl, and it is assumed that Fe⁰ is the species reducing H⁺ to form H₂ under acid conditions. As a result, electrons available in both types of particles were reported as the mass of Fe⁰. There is a 1:1 molar ratio between Fe⁰ and hydrogen (eq 4):



A measured mass of particles was added to 160 mL reactors containing 10 mL of acid, capped, and shaken for 5 h. Evolved H₂ was quantified by GC/TCD as described above. The reported Fe⁰ content of the nanoparticles was obtained from four replicate measurements. Errors reported are ± 1 standard deviation.

Particle Efficiency. Particle efficiency is defined here as the fraction of the Fe⁰ in the particles that is used to dechlorinate TCE. The electrons needed per mole of TCE dechlorinated depend on the products formed so values for n and m in eq 2 are reaction specific. For example, the reduction of TCE to ethane requires 8 electrons ($n = 8$) and 5 protons ($m = 5$):



Values of n for each of the observed hydrocarbon products are 6, 4, 8, 6, 7, and 6.7 for ethene, acetylene, ethane, butylenes, butane, and hexane, respectively. For a mixture of products, the value for n is calculated using eq 6:

$$n = \sum_i n_i p_i \quad (6)$$

where n_i is the coefficient for a single reaction (e.g., $n_i = 6$ for ethene), and p_i is the fraction of each product in a given experiment at the end of the reaction. The efficiency is calculated using eq 7:

$$\epsilon = \frac{(M_0 - M_f)n}{2N_0} \quad (7)$$

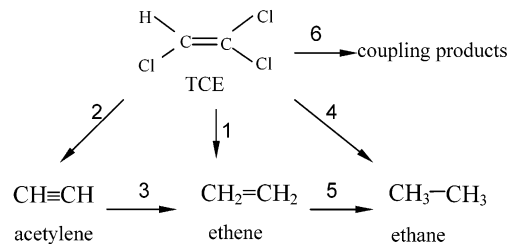


FIGURE 1. Reported reaction pathways for TCE and reaction intermediates in abiotic TCE dechlorination. Numbering corresponds to rate constants in Table 3.

TABLE 1. Properties of Fresh Nanoparticles before Reaction

	avg primary particle size (nm)	shape	boron (wt %)	specific surface area (m ² /g)	initial Fe ⁰ content (wt %)
Fe/B	30–40	spherical	5	36.5	97 \pm 8
RNIP	40–60	spheroid	<10 ⁻⁴ ^a	23	26.9 \pm 0.3

^a Based on information from Toda, Kyogo.

where M_0 is the initial moles of TCE in the reactor, M_f is the final moles of unreacted TCE at the end of reaction, and N_0 is the initial moles of Fe⁰ added to the reactor. It is assumed that the product ratios measured are representative of the total products formed even though carbon mass balances of 85–92% were achieved in the experiments.

Reaction Rates. The reactivity of each particle type was tested under two specific conditions. One set of experiments used a high iron to TCE ratio [low TCE concentration (4.4 mg/L) and an excess of Fe⁰ (~1.9 g/L)]. These experiments were of short duration (hours) to minimize deactivation or changes in the particle surface properties of the iron during the reaction. A second set of experiments used a low iron to TCE ratio [high TCE concentration (290 mg/L) and a limited Fe⁰ mass (~0.36 g/L)]. Excess TCE ensures that all the Fe⁰ would be consumed if it were accessible. Since less iron was used in these experiments, they typically lasted for several days. A third set of experiments used the same iron-limited conditions but with a pure H₂ headspace rather than argon. In control experiments without Fe⁰ particles, it was demonstrated that other loss mechanisms (e.g., photodegradation, adsorption, leakage) were negligible.

The TCE transformation rates for each particle type were evaluated using a kinetic modeling software package, Scientist, v.2.01 (Micromath, St. Louis, MO). Selected reaction pathways for RNIP and Fe/B from Figure 1 are hypothesized and evaluated based on the quality of fit to the experimental data. The loss of TCE and the formation of products were fit concurrently. Mass transfer resistance at the vapor/liquid interface was not considered as these phases are assumed to be in equilibrium (26).

Results

Particle Characterization. The properties of Fe/B and RNIP are provided in Table 1. The reported sizes were determined from at least five different TEM images. The size and specific surface area of Fe/B are similar to those reported in the literature (13, 16) despite minor differences in the iron synthesis method. The Fe/B has a higher initial Fe⁰ content (97 \pm 8%) than the RNIP (26.9 \pm 0.3%). The measured Fe⁰ content of RNIP is lower than the 60% Fe⁰ specified by the manufacturer, but this is probably because the particles had been slowly corroding to form H₂ during the 7 months they were stored in water before use.

Both particles show a distinct core/shell structure before reaction (Figure 2a,c). The core/shell morphology of RNIP

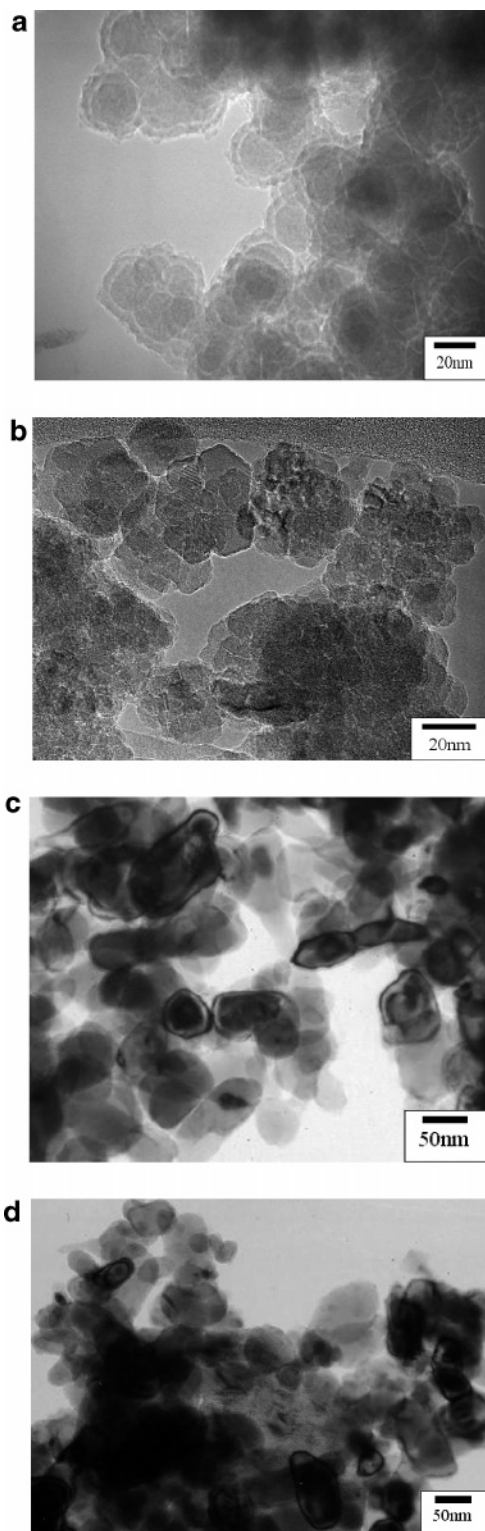


FIGURE 2. ARM image of Fe/B: (a) before reaction and (b) after reaction. TEM image of RNIP: (c) before reaction and (d) after reaction.

is consistent with the manufacturer's specifications. Lattice distances of 0.144, 0.112, 0.107, and 0.087 nm from ED of Fe/B and 0.203, 0.118, 0.101, and 0.091 nm from ED of RNIP are consistent with the ED patterns expected for bcc Fe⁰. No iron oxide phases were identified for Fe/B with ED. An oxygen-EELS map of Fe/B (not shown) reveals that oxygen atoms are concentrated in the shell of the particles, indicating that the shell is an oxide or oxyhydroxide of some sort. ED patterns from RNIP indicate Fe₃O₄ as the only iron oxide;

TABLE 2. Final Reaction Products

		Fe/B (%) ^a		RNIP (%)	
		excess iron	iron limited	excess iron	iron limited
1-C	methane	trace ^b	0.7	nd	nd
2-C	ethene	nd ^c	0.5	74.5	7.8
	acetylene	nd	nd	0	84.3
3-C	ethane	80	70.0	20.9	trace
	propylene	0.55	1.6	trace	0.6
	propane	1.7	2.4	trace	trace
4-C	1-butylene	1.4	2.1	2.7	1.5
	2-butylene	3.9	4.4	0.7	1.0
5-C	butane	7.4	9.0	0.8	1
	5-carbons	0.8	2.3	trace	1
6-C	6-carbons	4.4	6.9	trace	trace
CP ^d	VC	nd	trace	nd	trace
	c-DCE	nd	trace	nd	0.6

^a Percent of TCE transformed (i.e., 2 mol of TCE = 1 mol of C₄H₁₀).

^b Trace indicates percentage less than 0.5% for hydrocarbons. ^c nd, not detected. ^d CP, chlorinated products.

this was confirmed by XRD. More diffuse diffraction patterns for Fe/B relative to RNIP particle suggests that the Fe⁰ and iron oxides in RNIP are more crystalline than in Fe/B.

Products and Reaction Rates. Under iron-limited conditions, Fe/B transformed TCE to non-chlorinated hydrocarbons, mostly even-numbered saturated alkanes (87.4%), but other saturated and unsaturated hydrocarbons were also detected (Table 2). Ethene was a reactive intermediate and transformed to ethane. No acetylene was detected. Vinyl chloride and c-DCE were detected as reactive intermediates in the reactor at very low levels and disappeared quickly. The final products were ethane (70%) and C3–C6 coupling products (~30%). A similar distribution was found for Fe/B using excess iron: 80% ethane and ~20% C3–C6 coupling products.

Under iron-limited conditions, RNIP transformed TCE primarily to two carbon unsaturated compounds, including acetylene (84.3%) and ethene (7.8%). All the hydrocarbon products observed using Fe/B were also observed with RNIP, but fewer were formed. Vinyl chloride and c-DCE were still present when TCE dechlorination ceased but accounted for only 0.04% and 0.6% of the TCE transformed, respectively. Using excess iron, acetylene was a reactive intermediate that transformed to ethene. The primary reaction products were ethene (74.5%) and ethane (20.9%).

TCE dechlorination and the major products formed are shown in Figures 3a–d. Rate constants determined from model fits of the data are given in Table 3. Fe/B displayed zero-order kinetics under iron-limited conditions, and pseudo-first-order kinetics using excess iron. No deactivation was apparent during the course of the reaction using Fe/B. In the iron-limited case, excess TCE remains after the available Fe⁰ is consumed. Minor deviations from zero-order behavior at the end of the reaction ($t > 2.5$ d) were not considered in the fitting data (Figure 3a). TCE dechlorination by RNIP displayed pseudo-first-order kinetics under both reaction conditions. Deactivation was not observed using excess iron but was observed in the iron-limited case. Possible origins of the different observation are discussed below.

Particle Efficiency. The efficiency (Table 4) of each particle was calculated using the data collected under iron-limited conditions. The accessible Fe⁰ remaining in the particles after reaction (based on H₂ evolution) was zero for both particle types; however, XRD spectra of RNIP after reaction contained peaks for Fe⁰, indicating that some inaccessible Fe⁰ remains in the particle. On the basis of the measured product distributions (Table 2), n is 7.5 for Fe/B and 4.2 for RNIP.

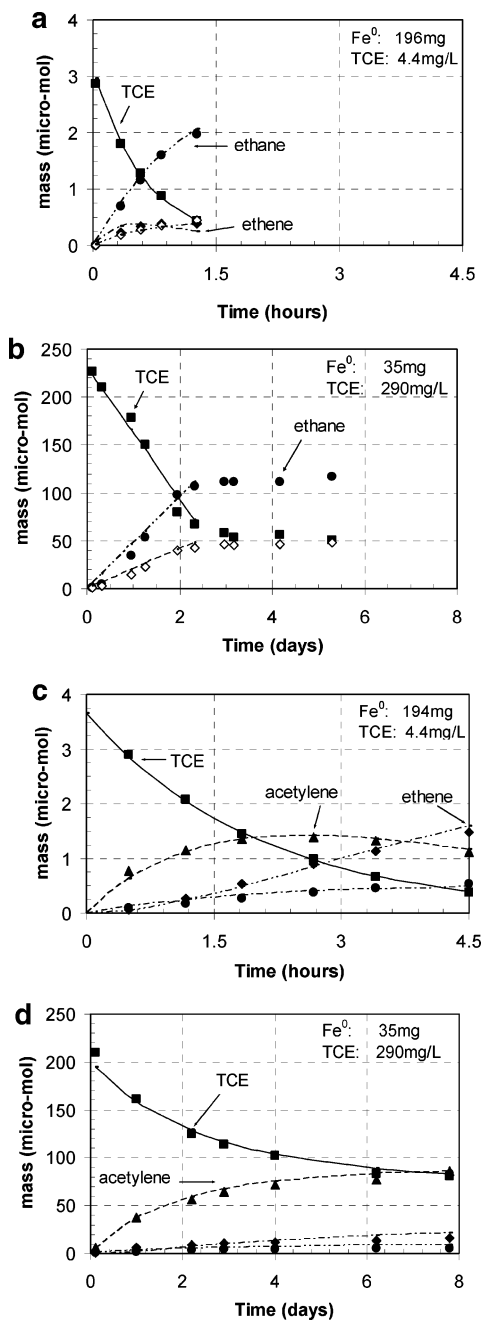


FIGURE 3. TCE dechlorination and major product formation using (a) Fe/B-excess iron; (b) Fe/B-iron limited; (c) RNIP-excess iron; and (d) RNIP-iron limited. Symbols: (■) TCE, (▲) acetylene, (◆) ethene, (●) ethane, (◇) coupling products (as C2). Lines represent model predictions based on the parameters in Table 3.

Using this value of n and the initial Fe^0 content of each particle (Table 1), the efficiency (ϵ) is 92% for Fe/B and 52% for RNIP.

H_2 Evolution and Its Effect on Particle Reactivity. The H_2 evolved from each particle type, expressed as the percentage of Fe^0 added to the reactor used to produce it, is shown in Figure 4. In DI water (no TCE), H_2 evolved after 3 d from Fe/B accounted for ~83% of the Fe^0 in the particle. The rate of H_2 evolution was rapid and constant in the first day ($31 \mu\text{mol of H}_2 \text{ L} \cdot \text{g}^{-1} \cdot \text{h}^{-1}$) and slowed at later times. All of the Fe^0 in the particle was consumed for H_2 evolution after 11 d. With TCE present (290 mg/L initial concentration), the H_2 concentration in the reactor reached a maximum (~20% of initial Fe^0) after 1 d but was ~zero by the end of the reaction. In DI water (no TCE), H_2 evolved from RNIP accounted for ~5.5% of the initial Fe^0 in the particles after 7 d and ~8.6%

TABLE 3. Model-Derived Rate Constants for TCE Dechlorination by Iron Nanoparticles

	Fe/B excess iron first-order ($\text{L} \cdot \text{h}^{-1} \cdot \text{m}^{-2}$)	iron-limited zero-order ($\text{mmol} \cdot \text{h}^{-1} \cdot \text{m}^{-2}$)
k_1^a	$5.4 \pm 2.1 \times 10^{-3}$	0
k_4	$2 \pm 7 \times 10^{-3}$	$1.4 \pm 0.4 \times 10^{-3}$
k_5	$1.9 \pm 1.4 \times 10^{-2}$	0
k_6	$6.8 \pm 2.8 \times 10^{-3}$	$5.9 \pm 2.3 \times 10^{-4}$
$k_{\text{TCE}} = k_1 + k_4 + k_6$	1.4×10^{-2}	2×10^{-3}

	RNIP excess iron first-order ($\text{L} \cdot \text{h}^{-1} \cdot \text{m}^{-2}$)	iron-limited first-order ($\text{L} \cdot \text{h}^{-1} \cdot \text{m}^{-2}$)
k_2	$2.6 \pm 0.2 \times 10^{-3}$	$3.3 \pm 0.06 \times 10^{-4}$
k_3	$1.9 \pm 0.2 \times 10^{-3}$	$1.6 \pm 1.3 \times 10^{-4}$
k_4	$4.6 \pm 0.6 \times 10^{-4}$	$0.28 \pm 0.16 \times 10^{-4}$
$k_{\text{TCE}} = k_2 + k_4$	3×10^{-3}	4×10^{-4}
k_d	0 (h)	0.012 ± 0.004 (h)

^a Subscripts correspond to transformations shown in Figure 1.
^b Errors are 95% confidence intervals.

TABLE 4. Nanoparticle Efficiency under Iron-Limited Conditions

	particle mass (mg)	Fe^0 mass (mg)	final TCE (mmol)	initial TCE (mmol)	n	efficiency (ϵ)	mmol of TCE dechlor/ g of Fe^0
Fe/B	40.4	39	0.054	0.22	7.5	92%	4.4
RNIP	136	36.6	0.051	0.21	4.2	52%	4.3

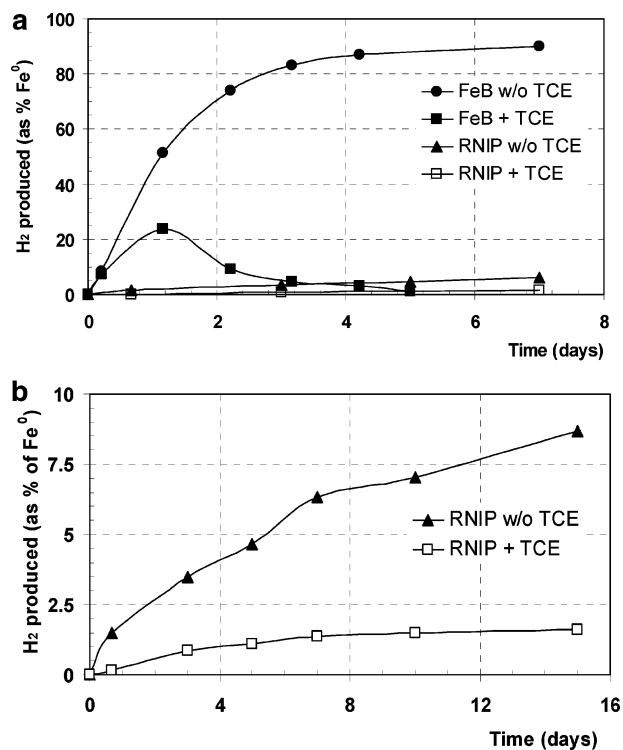


FIGURE 4. H_2 production with and without TCE: (a) both Fe/B and RNIP and (b) RNIP on an enlarged scale. Lines are interpolated (not fit) and only meant to guide the eye.

after 15 d. The rate of H_2 evolution appeared constant ($0.1 \mu\text{mol of H}_2 \text{ L} \cdot \text{g}^{-1} \cdot \text{h}^{-1}$) after 3 d. With TCE present (290 mg/L initial concentration), H_2 evolution was decreased by ~75%

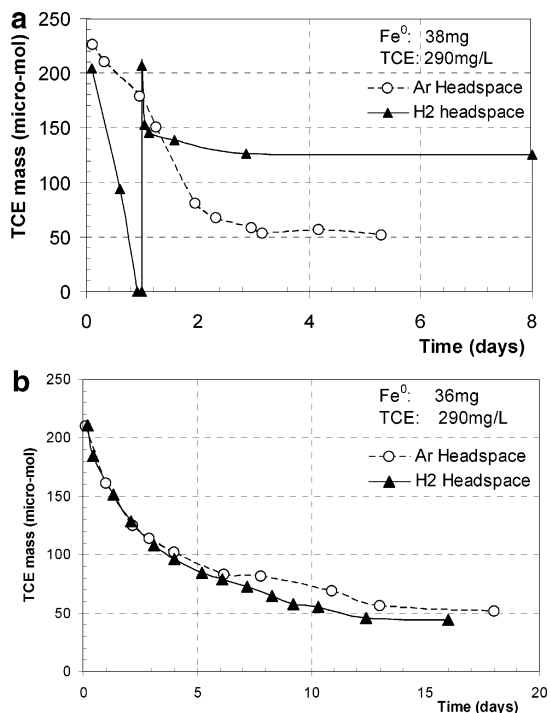


FIGURE 5. TCE dechlorination in Ar and H₂ headspaces: (a) Fe/B and (b) RNIP. Lines are interpolated (not fit) and only meant to guide the eye.

and stopped after 10 d. H₂ accumulated in the reactor and accounted for only ~2% of the initial Fe⁰ in the particles when TCE dechlorination ceased.

Experiments conducted using a H₂ headspace rather than argon are shown in (Figure 5a,b). For Fe/B, TCE disappeared in 22 h with a H₂ headspace as compared to ~72 h with an argon headspace. A second spike of TCE was added and ~40% of this spike was also degraded before the reaction stopped. The observed product distribution was nearly the same as for Fe/B using excess iron (Table 2). The moles of TCE reduced using a H₂ headspace was ~180% of the moles of TCE reduced using argon headspace, and given the similar products observed ($n = 7.7$), ~80% more TCE was reduced than the mass of Fe⁰ added to the reactor could have afforded assuming 2 mole of e⁻/mol of Fe⁰. No change in the reaction rate was observed for the RNIP using a H₂ headspace (Figure 5b).

Discussion

Reaction Rates and Products. Fe/B. Using excess iron the TCE dechlorination kinetics could be adequately modeled assuming direct pathways to radical coupling products (pathway 6), ethene (pathway 1), and ethane (pathway 4), and a pathway from ethene to ethane (pathway 5). The surface area normalized pseudo-first-order TCE dechlorination rate constant ($k_{TCE} = k_1 + k_4 + k_6$, Table 3) for Fe/B using excess iron ($1.4 \times 10^{-2} \text{ L}\cdot\text{h}^{-1}\cdot\text{m}^{-2}$) is higher than those reported for iron filings (10^{-4} – $10^{-3} \text{ L}\cdot\text{h}^{-1}\cdot\text{m}^{-2}$) (20) and for nanoscale iron ($\sim 10^{-3} \text{ L}\cdot\text{h}^{-1}\cdot\text{m}^{-2}$) (13, 16), though not as high as those reported for Ni–Fe ($9.8 \times 10^{-2} \text{ L}\cdot\text{h}^{-1}\cdot\text{m}^{-2}$) (16). The higher rate constant relative to that of iron filings could be due to the presence of B (5 wt %, ~16 at. %) if an Fe–B alloy or Fe–B oxide is formed and significantly alters the electrochemical properties of the particles. The higher reactivity as compared to other unmodified nanoscale iron (synthesized by borohydride reduction of dissolved iron) could be a result of the slight modification of particle synthesis. The physical characteristics of the particles (specific surface area, particle size and shape) are not likely to be responsible for the increased reactivity as they are very similar to those previously reported

(13, 16). Rather, the different Fe²⁺(aq) and NaBH₄(aq) concentrations, NaBH₄/Fe²⁺ ratio, solution pH, and rate of NaBH₄ addition (18) yielded a higher boron content (27), which could affect the particle properties. The saturated reaction products formed from Fe/B are more similar to those reported for bimetallics (Pd–Fe and Ni–Fe) and Pd-catalyzed TCE dechlorination (21) than for iron filings. This indicates a higher rate of hydrogenation compared to iron filings. More C3–C6 coupling products are formed from Fe/B than from a Pd catalyst. A catalytic reaction pathway, if active, could explain the high hydrogenation activity and the observed saturated products.

The pseudo-first-order kinetics observed using excess iron (low TCE concentration) are consistent with previous studies using nanoiron and bimetallic nanoparticles (16). The shift to zero-order kinetics under iron-limited conditions (high TCE concentration) has been observed for TCE dechlorination by iron filings and implies Langmuir–Hinshelwood–Hougen–Watson-type kinetics and strong binding of TCE to the iron surface (5). The absence of deactivation during TCE dechlorination by Fe/B suggests that the iron oxide or iron oxyhydroxide shell remains reactive throughout the reaction or that the particles are continuously dissolving during the reaction (shrinking particle model) to maintain fresh active sites. This contradicts the common conceptual model depicting growth of a passive and relatively insoluble iron oxide layer around the Fe⁰ core that inhibits the TCE dechlorination reaction (28).

RNIP. In contrast to Fe/B, TCE dechlorination by RNIP was adequately modeled assuming β -elimination (pathways 2 and 3) and a direct pathway to ethane (pathway 4). RNIP displayed pseudo-first-order reaction kinetics at both the high and low TCE/Fe ratios. This implies that TCE is only weakly adsorbed to reactive sites on the iron surface, that there is an abundance of reactive sites, or that some other factor (e.g., electron transport across the Fe₃O₄ shell) controls the rate of TCE dechlorination. The surface area normalized TCE reaction rate constant using excess iron is very similar to the rates for iron filings reported in the literature (10^{-4} – $10^{-3} \text{ L}\cdot\text{h}^{-1}\cdot\text{m}^{-2}$). The formation of acetylene and ethene as reactive intermediates and production of only minor amounts of C3–C6 coupling products are consistent with the β -elimination pathway previously reported (5), but here acetylene is less reactive because significant quantities are measured during the reaction. The order of magnitude lower TCE dechlorination rate constant measured under iron-limited (high [TCE]) conditions is consistent with TCE dechlorination by iron filings (5) and may be due to inhibition by acetylene. Acetylene, at concentrations much lower than observed here, was found to inhibit the rate of dechlorination of t-DCE by an order of magnitude using iron filings (5). The final products (ethene, ethane, and traces of coupling products) formed are also consistent with TCE dechlorination by iron filings reported in the literature (4, 5), suggesting that TCE dechlorination by RNIP is very similar to iron filings.

Unlike Fe/B, RNIP showed evidence of deactivation (first-order deactivation rate constant, $k_d = 0.29/\text{d}$) under iron-limited conditions. This is probably because the Fe₃O₄ shell grows during the reaction and hinders electron transport from the core to the exterior of the particle where TCE is degraded. This is consistent with the accepted conceptual model for iron filings. TEM images of RNIP after reaction under iron-limited conditions (Figure 2d) shows that the particle morphology after reaction is not considerably different from the fresh particles. This would be expected for a particle with an insoluble Fe₃O₄ shell and a reactive (shrinking) core. The increase of the Fe₃O₄ shell thickness during reaction may also limit accessibility to the Fe⁰ core in RNIP.

Particle Efficiency. *Fe/B.* The high electron efficiency (92%) of Fe/B for TCE dechlorination, the absence of detectable H₂ at the end of the reaction, and the absence of detectable Fe⁰ in the particles after reaction indicates that all of the Fe⁰ in these particles is used to dechlorinate TCE. Also, the Fe/B after reaction under iron-limited condition (Figure 2b) no longer has a core shell morphology. This again suggests that the iron oxide or iron hydroxide layer making up the shell never grows thick enough to hinder electron transport across the shell and slow the reaction or possibly that the particles are dissolving during the reaction and then recrystallizing. The fate of Fe/B during reaction is still under investigation.

RNIP. The electron efficiency of the RNIP (52%) under iron limited condition is lower than for Fe/B. This is in part due to the accumulation of H₂ in the reactor (2%), but primarily because some Fe⁰ (46%) is inaccessible. XRD peaks for Fe⁰ were observed in spent RNIP, indicating that Fe⁰ remained in the particle core. RNIP after the reaction did not evolve H₂ when digested in HCl, however, and some of the spent particles were not dissolved after 7 d in concentrated HCl. Fresh particles were completely digested after only 5 h. The Fe₃O₄ shell most likely grew thick enough to make Fe⁰ in the core inaccessible, but it remains unclear why Fe⁰ in the core is insoluble in concentrated HCl.

The lower value of *n* for RNIP (6.4) as compared to Fe/B (7.8) using excess iron is a result of the less saturated final products formed (ethene vs ethane). This implies that RNIP can dechlorinate 22% more TCE than Fe/B if all the Fe⁰ in the particles was used. Under iron-limited conditions this increases as *n* for RNIP and Fe/B are 4.2 and 7.5, respectively. If the iron to TCE ratio at TCE DNAPL-impacted sites results in iron limited conditions (likely if the source area is targeted), RNIP could dechlorinate up to 79% more TCE than Fe/B if all the Fe⁰ in the particles was used. Considering both the products formed (*n*) and the accessibility of Fe⁰ in the particles (efficiency), the mass of TCE dechlorinated per unit mass of Fe⁰ is similar for RNIP and Fe/B (Table 4). In a field application, other potential oxidants will be present (e.g., O₂, nitrate; 29) and the impact of these compounds on particle efficiency must also be considered.

H₂ Evolution and its Effect on Particle Reactivity. *Fe/B.* The appearance of H₂ as a reactive intermediate during TCE dechlorination indicates that it can be utilized after it is generated (Figure 4a). The higher TCE dechlorination rate for Fe/B in a H₂ headspace and the fact that ~80% more TCE was reduced than could be attributed to Fe⁰ demonstrate that Fe/B can catalyze the aqueous phase hydrodechlorination of TCE using H₂ as the reductant, despite the lack of a noble or transition metal catalyst. Noble metals (e.g., Pd) typically catalyze this reaction (21, 30); however, amorphous Fe–B and Ni–B ribbons prepared by rapid quenching could catalytically hydrogenate CO to C₁–C₃ hydrocarbons using H₂ gas (31, 32). Furthermore, Fe–Ni–B and Ni–B amorphous alloy synthesized from reduction of Fe(II)/Ni(II) or Ni(II) by KBH₄ have demonstrated catalytic hydrogenation of unsaturated organic compounds (33, 34). On the basis of these reports, it is likely that an Fe–B alloy is the catalytic species, but this is under further investigation. The decrease in H₂ evolution with TCE present as compared to deionized water (Figure 4a) may be due to the rapid consumption of H₂ in the catalytic reaction but could also be due to inhibition from TCE. Wang and Farrell (35) used electrochemical impedance spectroscopy to demonstrate that adsorbed atomic H (H⁺ + e⁻ → H*) tends to react with adsorbed TCE instead of combining to form H₂ gas. The high proportion of coupling products (~20–30%) indicates that another reaction pathway also exists, as fewer C3–C6 coupling products have been observed using a Pd catalyst (21).

RNIP. Adding H₂ to the reactor did not increase the TCE dechlorination reaction rate for RNIP indicating that H₂ does not play an important role. The lower H₂ evolution rate for RNIP as compared to Fe/B suggests that the amount of adsorbed H (if proportional to H₂ evolved) may be lower and may be limiting the TCE dechlorination rate. It has been demonstrated that the availability of adsorbed H was the limiting factor for TCE dechlorination by Ni–Fe bimetallics (16).

Physical and Chemical Properties Responsible for the Observed Differences. Considering the similar particle size and surface area for the two types of nanoparticles, differences in the particle composition, particularly the presence of boron, and the shell thickness are the most likely cause for the observed differences between the two particle types. Rapid TCE dechlorination and the absence of deactivation are attractive properties of Fe/B, but these particles may not be practical for in situ application because the rapid H₂ evolution would cause these particles to “burn out” prior to reaching their target. It may be possible to protect the Fe⁰ core of Fe/B using surface coatings other than noble metals, such as polymers. The thicker and more crystalline Fe₃O₄ shell of RNIP slows the TCE dechlorination rate and makes some Fe⁰ inaccessible, but the observed TCE dechlorination rates afforded by RNIP are likely to be rapid enough for in situ application. The Fe₃O₄ shell also decreases the reaction rate with water and protects the Fe⁰ core until it is delivered to the target area (RNIP stored in water remained active for more than 7 months). Both particle types have some desirable properties, and combining the desirable characteristics of each could provide optimal Fe⁰ nanoparticles for subsurface remediation of TCE.

Acknowledgments

This research was funded in part by the Office of Science (BER), U.S. Department of Energy, Grant DE-FG07-02ER63507, and in part by the U.S. EPA (R830898). Although the research described in this paper has been funded by the United States Environmental Protection Agency, it has not been subjected to the Agency's required peer and policy review and therefore does not necessarily reflect the views of the Agency, and no official endorsement should be inferred. Any opinions, findings, and conclusions or recommendations expressed in this material are those of the authors and do not necessarily reflect the views of the Department of Energy. The authors thank Prof. Krzysztof Matyjaszewski and the rest of the EMSP project team at CMU for insightful and helpful discussions. The authors also thank Dr. Christopher Kim (LBNL) and Dr. Yuhang Cheng (Carnegie Mellon University) for performing the EELS and TEM and Prof. Greg Rohrer for the use of his GC/TC/D.

Supporting Information Available

Detailed synthesis steps for the nanoscale iron used in this study. This material is available free of charge via the Internet at <http://pubs.acs.org>.

Literature Cited

- Gillham, R. W.; O'Hannesin, S. F. Enhanced degradation of halogenated aliphatics by zero-valent iron. *Ground Water* **1994**, *32*, 958–967.
- Matheson, L. J.; Tratnyek, P. G. Reductive dehalogenation of chlorinated methanes by iron metal. *Environ. Sci. Technol.* **1994**, *28*, 2045–2053.
- Roberts, A. L.; Totten, L. A.; Arnold, W. A.; Burris, D. R.; Campbell, T. J. Reductive elimination of chlorinated ethylenes by zero-valent metals. *Environ. Sci. Technol.* **1996**, *30*, 2654–2659.
- Orth, W. S.; Gillham, R. W. Dechlorination of trichloroethene in aqueous solution using Fe⁰. *Environ. Sci. Technol.* **1996**, *30*, 66–71.

- (5) Arnold, W. A.; Roberts, A. L. Pathway and kinetics of chlorinated ethylene and chlorinated acetylene reaction with Fe(0) particles. *Environ. Sci. Technol.* **2000**, *34*, 1794–1805.
- (6) Su, C.; Puls, R. W. Kinetics of trichloroethene reduction by zerovalent iron and tin: pretreatment effect, apparent activation energy, and intermediate products. *Environ. Sci. Technol.* **1999**, *33*, 163–168.
- (7) Johnson, T. L.; Fish, W.; Gorby, Y. A.; Tratnyek, P. G. Degradation of carbon tetrachloride by iron metal: complexation effects on the oxide surface. *J. Contam. Hydrol.* **1998**, *29*, 379–398.
- (8) Gaspar, D. J.; Lea, A. S.; Engelhard, M. H.; Baer, D. R. Evidence for localization of reaction upon reduction of carbon tetrachloride by granular iron. *Langmuir* **2002**, *18*, 7688–7693.
- (9) Gotpagar, J.; Lyuksyutov, S.; Cohn, R.; Grulke, E.; Bhattacharyya, D. Reductive dehalogenation of trichloroethylene with zerovalent iron: surface profiling microscopy and rate enhancement studies. *Langmuir* **1999**, *15*, 8412–8420.
- (10) Elliott, D. W.; Zhang, W.-X. Field assessment of nanoscale bimetallic particles for groundwater treatment. *Environ. Sci. Technol.* **2001**, *35*, 4922–4926.
- (11) Geiger, C. L.; Clausen, C. A.; Brooks, K.; Coon, C.; Huntley, C.; Filipek, L.; DeVor, R.; Krug, T.; O'Hara, S.; Majors, D.; Quinn, J. Remediation of DNAPLs using emulsified zero-valent iron: laboratory and field results. *ACS Symp. Ser., Div. Environ. Chem.* **2003**, No. 43, 939–944.
- (12) Schrick, B.; Hydutsky, B. W.; Blough, J. L.; Mallouk, T. E. Delivery vehicles for zerovalent metal nanoparticles in soil and groundwater. *Chem. Mater.* **2004**, *16*, 2187–2193.
- (13) Wang, C.-B.; Zhang, W.-X. Synthesizing nanoscale iron particles for rapid and complete dechlorination of TCE and PCBs. *Environ. Sci. Technol.* **1997**, *31*, 2154–2156.
- (14) Lien, H.-L.; Zhang, W.-X. Nanoscale iron particles for complete reduction of chlorinated ethenes. *Colloid Surf. A* **2001**, *191*, 97–105.
- (15) Lien, H.-L.; Zhang, W.-X. Transformation of chlorinated methanes by nanoscale iron particles. *J. Environ. Eng. ASCE* **1999**, *125*, 1042–1047.
- (16) Schrick, B.; Blough, J. L.; Jones, A. D.; Mallouk, T. E. Hydrodechlorination of trichloroethylene to hydrocarbons using bimetallic nickel–iron nanoparticles. *Chem. Mater.* **2002**, *14*, 5140–5147.
- (17) Zhang, W.-X. Nanoscale iron particles for environmental remediation: an overview. *J. Nanopart. Res.* **2003**, *5*, 323–332.
- (18) Ponder, S. M.; Darab, J. G.; Mallouk, T. E. Remediation of Cr(VI) and Pb(II) aqueous solutions using supported, nanoscale zerovalent iron. *Environ. Sci. Technol.* **2000**, *34*, 2564–2569.
- (19) Ponder, S. M.; Darab, J. G.; Bucher, J.; Caulder, D.; Craig, I.; Davis, L.; Edelstein, N.; Lukens, W.; Nitsche, H.; Rao, L.; Shuh, D. K.; Mallouk, T. E. Surface chemistry and electrochemistry of supported zerovalent iron nanoparticles in the remediation of aqueous metal contaminants. *Chem. Mater.* **2001**, *13*, 479–486.
- (20) Johnson, T. L.; Scherer, M. M.; Tratnyek, P. G. Kinetics of halogenated organic compound degradation by iron metal. *Environ. Sci. Technol.* **1996**, *30*, 2634–2640.
- (21) Lowry, G. V.; Reinhard, M. Hydrodehalogenation of 1- to 3-carbon halogenated organic compounds in water using a palladium catalyst and hydrogen gas. *Environ. Sci. Technol.* **1999**, *33*, 1905–1910.
- (22) Uegami, M.; Kawano, J.; Okita, T.; Fujii, Y.; Okinaka, K.; Kakuya, K.; Yatagai, S. Iron particles for purifying contaminated soil or ground water, process for producing the iron particles, purifying agent comprising the iron particles, process for producing the purifying agent and method of purifying contaminated soil or ground water. U.S. Patent Application 20030217974A1, 2003.
- (23) Heron, G.; Christensen, T. H.; Enfield, C. G. Henry's law constant for trichloroethylene between 10 and 95°C. *Environ. Sci. Technol.* **1998**, *32*, 1433–1437.
- (24) U.S. EPA. *Engineered Approaches to In Situ Bioremediation of Chlorinated Solvents: Fundamentals and Field Applications*; EPA 542-R-00-008; U.S. Government Printing Office: Washington, DC, 2000.
- (25) Schwarzenbach, R. P.; Gschwend, P. M.; Imboden, D. M. *Environmental Organic Chemistry*, 2ed.; John Wiley & Sons: Hoboken, NJ, 2003; pp 1198–1208.
- (26) Burris, D. R.; Delcomyn, C. A.; Smith, M. H.; Roberts, A. L. Reductive dechlorination of tetrachloroethylene and trichloroethylene catalyzed by Vitamin B12 in homogeneous and heterogeneous systems. *Environ. Sci. Technol.* **1996**, *30*, 3047–3052.
- (27) Shen, J.; Li, Z.; Yan, Q.; Chen, Y. Reactions of bivalent metal ions with borohydride in aqueous solution for the preparation of ultrafine amorphous alloy particles. *J. Phys. Chem.* **1993**, *97*, 8504–8511.
- (28) Farrell, J.; Kason, M.; Melitas, N.; Li, T. Investigation of the long-term performance of zero-valent iron for reductive dechlorination of trichloroethylene. *Environ. Sci. Technol.* **2000**, *34*, 514–521.
- (29) Alowitz, M. J.; Scherer, M. M. Kinetics of nitrate, nitrite, and Cr(VI) reduction by iron metal. *Environ. Sci. Technol.* **2002**, *36*, 299–306.
- (30) Lowry, G. V.; Reinhard, M. Pd-catalyzed TCE dechlorination in water: effect of [H₂](aq) and H₂ utilizing competitive solutes on the TCE dechlorination rate and product distribution. *Environ. Sci. Technol.* **2001**, *35*, 696–702.
- (31) Yokoyama, A.; Komiyama, H.; Inoue, H. The hydrogenation of carbon monoxide by amorphous ribbons. *J. Catal.* **1981**, *68*, 355–361.
- (32) Molnar, A.; Smith, G. V.; Bartok, M. New catalytic materials from amorphous metal alloys. *Adv. Catal.* **1989**, *36*, 329–383.
- (33) Deng, J.; Yang, J.; Sheng, S.; Chen, H.; Xiong, G. The study of ultrafine Ni–B and Ni–P amorphous alloy powders as catalysts. *J. Catal.* **1994**, *150*, 434–438.
- (34) Yu, Z.; Qiao, M.; Li, H.; Deng, J. Preparation of amorphous Ni–Co–B alloys and the effect of cobalt on their hydrogenation activity. *Appl. Catal. A* **1997**, *163*, 1–13.
- (35) Wang, J.; Farrell, J. Investigating the role of atomic hydrogen on chloroethene reactions with iron using Tafel analysis and electrochemical impedance spectroscopy. *Environ. Sci. Technol.* **2003**, *37*, 3891–3896.

Received for review May 31, 2004. Revised manuscript received September 7, 2004. Accepted September 27, 2004.

ES049195R